

See discussions, stats, and author profiles for this publication at: <https://www.researchgate.net/publication/267757086>

Novel Capsaicin Analogues as Potential Anticancer Agents: Synthesis, Biological Evaluation, and In Silico Approach

ARTICLE *in* ARCHIV DER PHARMAZIE · OCTOBER 2014

Impact Factor: 1.53 · DOI: 10.1002/ardp.201400233 · Source: PubMed

CITATIONS

2

READS

47

11 AUTHORS, INCLUDING:



[Kerly Fernanda Mesquita Pasqualoto](#)

Instituto Butantan

60 PUBLICATIONS 429 CITATIONS

SEE PROFILE



[José Alexandre Marzagão Barbuto](#)

University of São Paulo

79 PUBLICATIONS 594 CITATIONS

SEE PROFILE



[Fanny Palace-Berl](#)

University of São Paulo

9 PUBLICATIONS 50 CITATIONS

SEE PROFILE



[Roberto Parise Filho](#)

University of São Paulo

24 PUBLICATIONS 64 CITATIONS

SEE PROFILE

Full Paper

Novel Capsaicin Analogues as Potential Anticancer Agents: Synthesis, Biological Evaluation, and *In Silico* Approach

Mariana C. F. C. B. Damião¹, Kerly F. M. Pasqualoto², Adilson K. Ferreira³, Sarah F. Teixeira³, Ricardo A. Azevedo³, José A. M. Barbuto^{3,4}, Fanny Palace-Berl⁵, Gilberto C. Franchi-Junior⁶, Alexandre E. Nowill⁶, Maurício T. Tavares¹, and Roberto Parise-Filho¹

¹ Department of Pharmacy, School of Pharmaceutical Sciences, University of São Paulo, São Paulo, SP, Brazil

² Biochemistry and Biophysical Laboratory, Butantan Institute, São Paulo, SP, Brazil

³ Laboratory of Tumor Immunology, Department of Immunology, Institute of Biomedical Sciences, University of São Paulo, São Paulo, SP, Brazil

⁴ Cell and Molecular Therapy Center (NUCEL-NETCEM), Faculty of Medicine, University of São Paulo, São Paulo, SP, Brazil

⁵ Department of Biochemical-Pharmaceutical Technology, School of Pharmaceutical Sciences, University of São Paulo, São Paulo, SP, Brazil

⁶ Onco-Hematological Child Research Center, Faculty of Medical Sciences, State University of Campinas, Campinas, SP, Brazil

A novel class of benzo[d][1,3]dioxol-5-ylmethyl alkyl/aryl amide and ester analogues of capsaicin were designed, synthesized, and evaluated for their cytotoxic activity against human and murine cancer cell lines (B16F10, SK-MEL-28, NCI-H1299, NCI-H460, SK-BR-3, and MDA-MB-231) and human lung fibroblasts (MRC-5). Three compounds (**5f**, **6c**, and **6e**) selectively inhibited the growth of aggressive cancer cells in the micromolar (μM) range. Furthermore, an exploratory data analysis pointed at the topological and electronic molecular properties as responsible for the discrimination process regarding the set of investigated compounds. The findings suggest that the applied designing strategy, besides providing more potent analogues, indicates the aryl amides and esters as well as the alkyl esters as interesting scaffolds to design and develop novel anticancer agents.

Keywords: Bioisosterism / Capsaicin analogues / Cytotoxic activity / Exploratory data analysis / Molecular modification

Received: June 9, 2014; Revised: July 28, 2014; Accepted: August 15, 2014

DOI 10.1002/ardp.201400233



Additional supporting information may be found in the online version of this article at the publisher's web-site.

Introduction

Cancer is the second leading cause of human death in developed and developing countries, accounting for nearly one in five deaths [1]. Although there are many therapeutic strategies, high systemic toxicity, low selectivity, and drug resistance are the main problems in the treatment of cancer. Therefore, to find new therapeutic targets for cancer and

discover novel potent and selective antineoplastic drugs can be considered as a big challenge for medicinal chemists [2–5]. Programmed cell death is a natural process to remove unwanted cells, such as those with potentially harmful mutations, aberrant substratum attachment, or alterations in cell-cycle control. Deregulation of apoptosis can disrupt the delicate balance between cell proliferation and cell death, and can lead to diseases, as cancer, for instance [6, 7]. In this regard, it is important to modulate the apoptotic signaling pathways to constitute a key event in the antitumor activities.

In the past few years, the potential of capsaicin for inducing apoptosis in a wide variety of tumors has been demonstrated [8–13], but its strong pungency and nociceptive activity [14] limit its application in food or medicinal fields. Capsaicin

Correspondence: Dr. Roberto Parise-Filho, Department of Pharmacy, School of Pharmaceutical Sciences, University of São Paulo, Prof. Lineu Prestes Avenue, 580, 05508-000 São Paulo, Brazil.

E-mail: roberto.parise@usp.br

Fax: +55 11 3091-3815

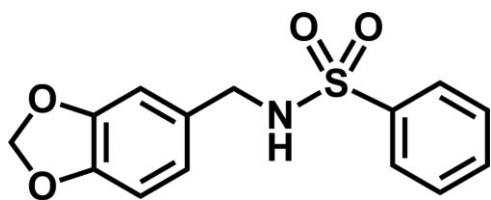


Figure 1. Chemical structure of RPF101.

might be considered as a potential lead, for instance, to the rational design of a novel class of antineoplastic drugs with improved pharmacokinetics and pharmacodynamics profiles.

Recently, our group reported the synthesis and antitumoral activity of RPF101 (Fig. 1), a structural analogue of capsaicin designed by applying the ligand-based strategy [15].

RPF101 was more potent than its prototype by inducing apoptosis and cell cycle arrest at the G2/M phase through disruption of the microtubule network in the MCF-7 breast cancer cells. In our efforts to develop more potent and selective anticancer agents, combined with the relevant and promising profile of RPF101, a novel series of benzo[1,3]dioxol-5-ylmethyl alkyl/aryl amides and esters were also designed through the ligand-based drug design (LBDD) strategy. Thereby, the amidic bond present in capsaicin was preserved (5a–f) or replaced by an isosteric ester group (6a–e) (Fig. 2).

Bioisosterism strategy is commonly used to improve therapeutic properties, such as potency, selectivity and pharmacokinetics of key compounds, or generate incremental innovation [16]. The replacement of amide bonds, particularly, by suitable bioisoster groups, which maintain similar geometric, electronic, or hydrogen bonding properties, has been well succeeded and extensively applied [17]. Additionally, the methylcatechol group was modified in order to achieve the 1,3-benzodioxole bicyclic system, which is a privileged structural feature present in anticancer agents, such as podophylotoxin and derivatives [18, 19]. Furthermore, the lipophilic chain was replaced by various alkyl/aryl groups to maintain the hydrophobic character on this specific region of the molecule.

The novel sets were synthesized and evaluated *in vitro* for their cytotoxicity in the following cell lines: Murine melanoma (B16F10), human melanoma (SK-MEL-28), human lung cancer (NCI-H1299 and NCI-H460), breast adenocarcinoma (SK-BR-3 and MDA-MB-231), and human lung fibroblast (MRC-5), through the MTT (3-[4,5-dimethylthiazol-2-yl]-2,5-diphenyl tetrazolium bromide) assay.

Herein, *in silico* studies, comprising molecular modeling and chemometric methods, were also carried out to (i) select the energetically favorable conformation of each compound and, then, (ii) calculate its molecular properties (electronic, steric, hydrophobic, topological, geometric), which were used

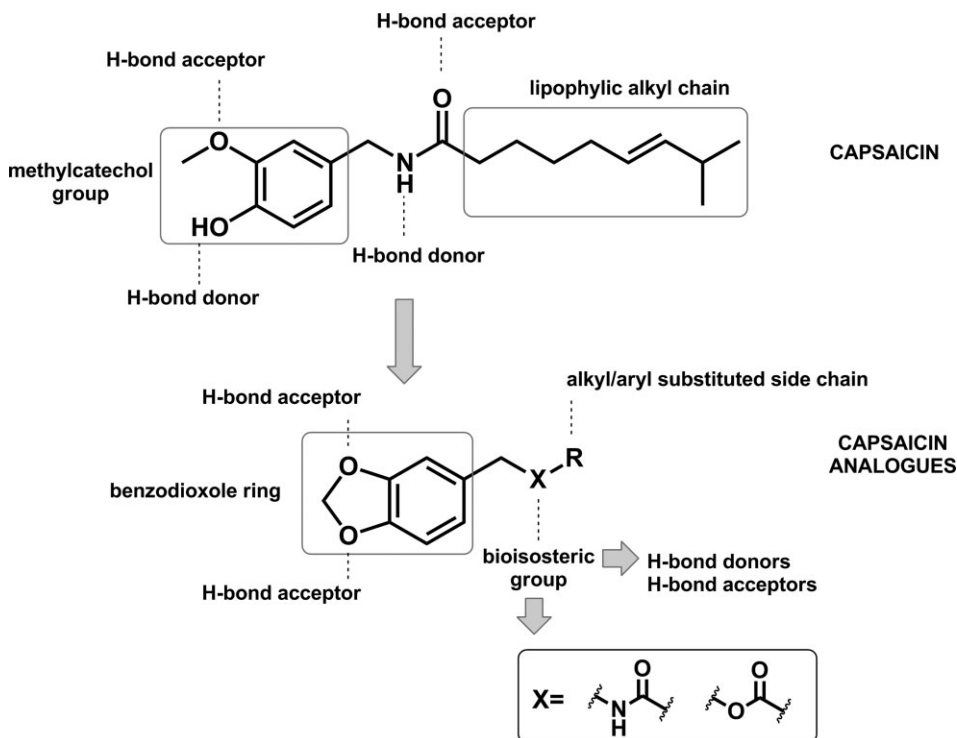


Figure 2. Chemical structure of capsaicin and general structure of capsaicin analogues.

to (iii) perform the exploratory data analysis (hierarchical cluster analysis, HCA, and principal components analysis, PCA) [20–22]. The findings were helpful to establish some qualitative structure–property relationships, since the calculated molecular properties are directly related to the compounds' chemical structures, which are responsible for the molecular recognition process.

Results and discussion

Chemistry

An efficient and simple two-step methodology was employed to obtain capsaicin analogues. Amide (**5a–f**) and ester (**6a–e**) products were synthesized by treatment of **3a–3j** with oxalyl chloride in CH_2Cl_2 , at room temperature for 2 h, followed by acylation of benzo[d][1,3]dioxol-5-ylmethanamine **1** and benzo[d][1,3]dioxol-5-ylmethanol **2**. Formation of acyl chlorides from carboxylic acids, for further acylation was applied due to its wide applicability and common use. In this regard, both synthetic procedures were suitable for amide and ester formation and provided satisfactory yields (values between 60% and 74%). The synthetic steps are depicted in Scheme 1 [23, 24].

Biological activity

Cell viability assay

The synthesized derivatives **5a–f**, **6a–e** were evaluated for their *in vitro* cytotoxic activity against a panel of tumor and non-tumor cells [murine melanoma (B16F10), human melanoma (SK-MEL-28), non-small cell lung cancer (NCI-H1299 and NCI-H460), breast adenocarcinoma (SK-BR-3 and MDA-MB-231), and human fetal lung fibroblasts (MRC-5)] in a range from 50.0 to 200.0 μM . The assays were carried out in triplicate, and

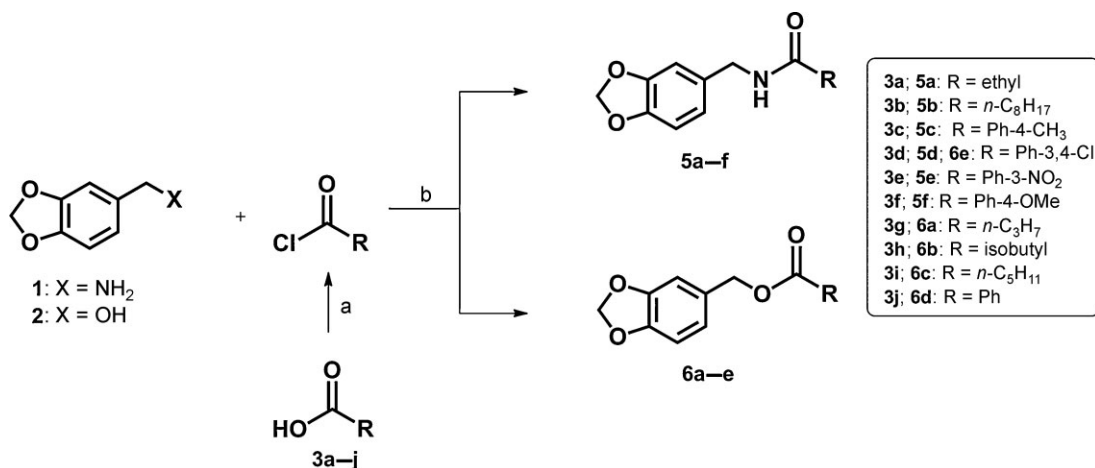
capsaicin was used as the standard compound. The biological endpoint was determined as the concentration, which causes fifty percent of cell growth inhibition (IC_{50}). The cytotoxicity did not differ greatly from the chemical nature and size of the substituent groups. Indeed, all compounds showed similar values of cytotoxicity. Over all, three compounds in particular [**5f** ($\text{R} = 4\text{-OMe-Ph}$), **6c** ($n\text{-hexanoyl}$), and **6e** ($\text{R} = 3,4\text{-Cl-Ph}$)] have shown promising cytotoxic profile when compared to capsaicin (see Table 1).

Regarding Table 1, the amide analogue **5f** (methoxyl group attached to the aromatic ring) induced cytotoxic effects on B16F10 and H1299 cells ($\text{IC}_{50} = 87$ and $187 \mu\text{M}$, respectively). These results reveal the methoxyl amide as the most promising compound of the set of capsaicin analogues.

Additionally, compound **5f** is more potent against B16F10 ($\text{IC}_{50} = 87 \mu\text{M}$) than the alkyl ester, **6c** ($n\text{-hexanoyl}$ analogue) ($\text{IC}_{50} = 130 \mu\text{M}$). The ester analogue (**6c**) contains a more flexible substituent group at the R position and was more effective against SK-MEL-28 ($\text{IC}_{50} = 85 \mu\text{M}$) cell line, differently from the other analogues (**5f** and **6e**) and the prototype, capsaicin. These results have suggested that the alkyl ester compound presents an interesting biological profile, mainly, against melanoma cell lines.

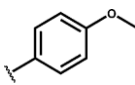
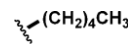
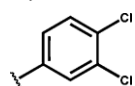
The ester analogue, **6e** (3,4-dichloro attached to the aromatic ring) induced preferentially cytotoxic effects in the H1299 cells ($\text{IC}_{50} = 172 \mu\text{M}$) in comparison to the prototype. However, **5f**, **6c**, and **6e** compounds were inactive in human non-small cell lung cancer (NCI-H460) and breast adenocarcinoma (SK-BR-3 and MDA-MB-231) cells.

Interestingly, compounds **5f**, **6c**, and **6e** did not present cytotoxicity against human fetal lung fibroblasts (MRC-5), indicating that these molecules exhibit a certain selective profile in comparison to capsaicin ($\text{IC}_{50} = 10 \mu\text{M}$). Then, our



Scheme 1. Synthetic route of benzo[d][1,3]dioxol-5-ylmethyl amides (**5a–f**) and esters (**6a–e**). Reagents and conditions: (a) oxalyl chloride, CH_2Cl_2 , cat. DMF, r.t., 2 h; (b) Et_3N , cat. DMAP, CH_2Cl_2 , 0°C , 24 h.

Table 1. Cytotoxic activity (IC_{50} μ M) of compounds **5f**, **6c**, and **6e**.

		Cell lines						
Compounds	R	B16F10	SK-MEL-28	NCI-H1299	NCI-H460	SK-BR-3	MDA-MB-231	MRC-5
		IC_{50} (μ M)	IC_{50} (μ M)	IC_{50} (μ M)	IC_{50} (μ M)	IC_{50} (μ M)	IC_{50} (μ M)	IC_{50} (μ M)
Capsaicin		117	≥ 200	≥ 200	120	75	48	10
5f		87	≥ 200	187	≥ 200	≥ 200	≥ 200	≥ 200
6c		130	85	≥ 200	≥ 200	≥ 200	≥ 200	≥ 200
6e		≥ 200	≥ 200	172	≥ 200	≥ 200	≥ 200	≥ 200

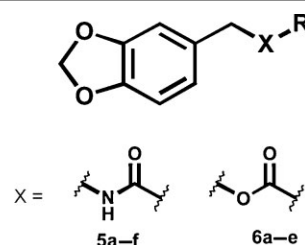
findings have indicated that the designing strategy applied here has produced more selective and active analogues than the prototype, capsaicin.

Additionally, the benzo[d][1,3]dioxol-5-ylmethyl aryl/alkyl capsaicin bioisosters, such as **5f** and **6c**, might be interesting scaffolds for optimization against lung cancer.

Molecular modeling approach

The purpose of the theoretical approach was to find energetically more favorable conformations for capsaicin and its analogues (**5a–f** and **6a–e**), calculate the molecular properties and, finally, provide some insights regarding structure–activity relationships by exploratory data analysis. Molecular dynamics (MD) simulations (1 ns at 310 K) of all compounds reached the thermodynamic equilibrium between 400,000 and 600,000 simulation steps. The lowest-energy conformer of each molecule was selected from the equilibrium region of the conformational ensemble profile (CEP). Additionally, root mean square deviation (RMSD) values between the atomic positions of the selected conformers and the atomic positions of the energy-minimized structures were computed as a criterion to verify whether the structural integrity was maintained after simulations. Higher RMSD values indicate loss of structural integrity during MD simulations if there is considered a crystallographic structure as template or reference [25].

The RMSD value found between the lowest-energy conformer and the initial energy-minimized structure of capsaicin was 0.53 Å and lower than 0.09 Å for its analogues. The higher



RMSD value found for capsaicin was already expected since the molecular model was built up using a crystallographic structure that shares little resemblance with the prototype.

The intramolecular energy contributions (i.e., thermodynamic properties) found for the selected lowest-energy conformations from MD simulation at 310 K were the following: Stretching (E_{STRETCH}), bending (E_{BEND}), torsional (E_{TORS}), Lennard–Jones or 1–4 interactions ($E_{1,4}$), van der Waals (E_{vdW}), electrostatic (E_{CHARGE}), hydrogen bonding (E_{HB}), and solvation (E_{SOLV}). The summation of all energy contributions, which correspond to the total potential energy (E_{TOT}), was also considered.

To the set of designed molecules, E_{TOT} values varied from 2.70 to 36.33 kcal/mol, of which capsaicin and **5b** presented higher (more positive) values (31.81 and 36.33 kcal/mol, respectively) than the other compounds. This fact reflects more degrees of freedom, once both molecules present a carbonic side chain of nine atoms (see Supplementary Information, Table S2).

Then, 48 descriptors or molecular properties of different nature were calculated (thermodynamic, hydrophobic, electronic, topological, geometric, and steric) for each compound. A table composed of 12 rows (samples plus capsaicin) and 48 columns (independent variables or descriptors or molecular properties) was generated and used as input for the exploratory data analysis (PCA and HCA). All calculated descriptors and their methods are shown in the Supplementary Information (Table S1).

Exploratory analysis

Exploratory data analysis allows the investigation of inter-samples relationships through either similarity indices, or linear combinations from the original data set. The findings can be used to establish structure–molecular property relationships, since the calculated descriptors are directly related to the compounds' chemical structure.

The unsupervised PCA aimed to correlate the descriptors to find other uncorrelated variables, the principal components (PCs), which can describe the information from the original data set [20, 21].

The PCA findings from exploratory data analysis are shown in Fig. 3. According to the factors selection (Fig. 3a), the two first factors or PCs discriminated more than sixty percent (61.93%) of total variance from the original data. PC1, or factor 1, explained 34.90% of total variance whereas PC2, or factor 2, described 27.03%. Also PC3, PC4, and PC5 discriminated

15.28%, 9.59%, and 6.92%, respectively, of total variance from the original data, meaning they did not influence significantly the samples separation process, and, then, were not considered for further discussion.

PC1, or factor 1, seems to be responsible for splitting the samples according to their isosteric functional groups. Amides, including capsaicin, were positioned at the positive side of PC1 axis whereas the ester analogues remained at the negative side. Compound **5a**, amide analogue with short side chain, is an exception to the pattern observed in factor 1.

Interestingly, PC2 or factor 2 has considered mostly the kind of substitution in the amide or ester bond position (R group), whether aryl or alkyl substituent group. Then, regarding PC2, the compounds were separated into three smaller groups: A, which presents amides with long side chains (capsaicin and **5b**); B that comprises ester analogues with aliphatic side chains (**6a**, **6b**, and **6c**); and C, which

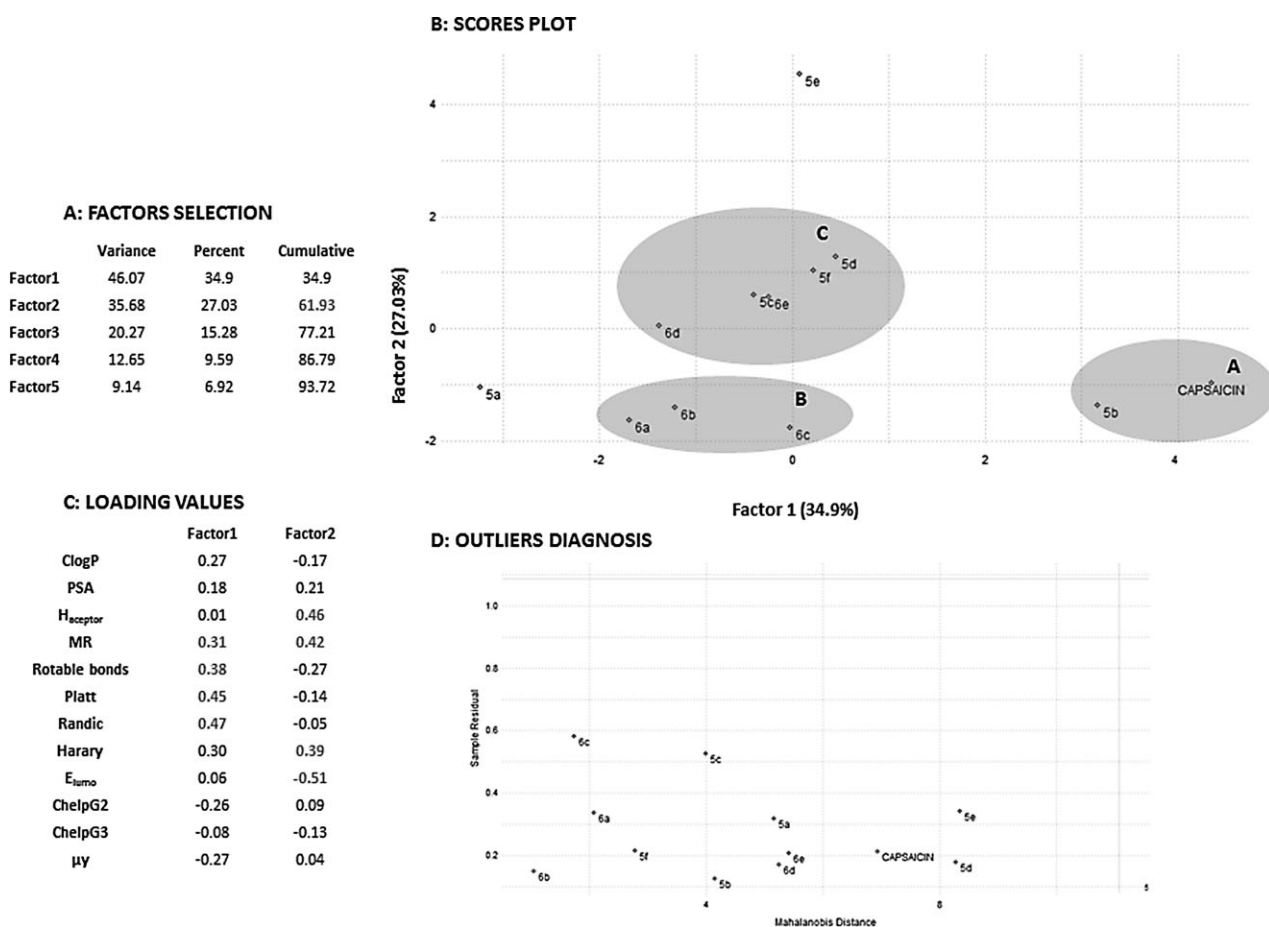


Figure 3. PCA findings: (a) Factors selection, factor 1 and 2 discriminated 61.93% of total variance from original data; (b) scores plot for PC1 (factor 1) versus PC2 (factor 2), the samples were classified mainly into three groups according to functionality and/or substitution [A (amides with long side chain: capsaicin and **5b**), B (alkyl ester analogues: **6a**, **6b**, and **6c**), and C (aryl amides and esters: **5d**, **5f**, **5c**, **6e**, and **6d**)]; (c) loading values for the calculated descriptors regarding factor (or PC) 1 and 2; (d) outliers diagnosis through the sample residuals versus Mahalanobis distance. The sample residual threshold (green line) is based upon 95% probability limit (set internally in Pirouette program).

contains the compounds with aromatic substituent groups (5d, 5f, 5c, 6e, and 6d). The amide analogues 5e (nitro-substituted) and 5a (short side chain) remained alone and more distant from the rest due to their structural features at the R position.

It is noteworthy that compounds 5f, 6c, and 6e, experimentally evaluated, were in B and C groups, and positioned closely to the PC1 axis. This information will be useful for the designing of new analogues, since molecules that are positioned around PC1 axis would be likely more promising against tumor cell lines since they share molecular properties with the three tested compounds.

The loadings' table, presented in Fig. 3c, provides information about which descriptors or molecular properties mostly influenced the samples discrimination. In PC1, or factor 1 (34.9%), topological (Randic index, Platt index, number of routable bonds) and steric/hydrophobic (molar refractivity, MR) molecular properties presented higher loading values (absolute values; >0.3). In PC2, or factor 2 (27.03%), electronic (the lowest unoccupied molecular orbital energy, E_{lumo}), topological (H_{acceptor} , Harary index) and steric/hydrophobic (MR) molecular properties influenced more the samples separation. Also, their loading values varied from 0.39 to 0.51 (absolute values).

Moreover, the plot of sample residual *versus* Mahalanobis distances [26] (Fig. 3d) indicated there were no outliers. The sample residual threshold (light green line) is based upon a 95% of confidence level interval set internally in Pirouette 3.11 [27]. The compounds did not exceed a threshold value, meaning the calculated properties were sufficient to describe the structural features of the entire data set.

Complementary findings were obtained for both methods, PCA and HCA, reinforcing particularly the discrimination pattern given by PC1 and PC2, as can be seen in the dendrogram of samples (Fig. 4). HCA analysis presented higher distinction between samples and classified them into four sub-clusters (A, B, C, and E) when a similarity cursor of 0.6 (dashed line) was considered as reference.

The compounds were grouped, in general, accordingly to their functional groups (ester or amide) and nature of side chain (alkyl or aryl). Considering ester analogues, compounds were mainly grouped into two clusters: A (68.8% similarity) and C (66.3% similarity). Cluster A was composed of alkyl esters and cluster C of aryl esters. Regarding amide analogues, compounds were grouped in cluster B (69.8% similarity) and E (64.1% similarity). Cluster B was composed by aryl amides substituted by electron donating groups (4- OCH_3 , 4- CH_3), while cluster E comprises amides with long alkyl

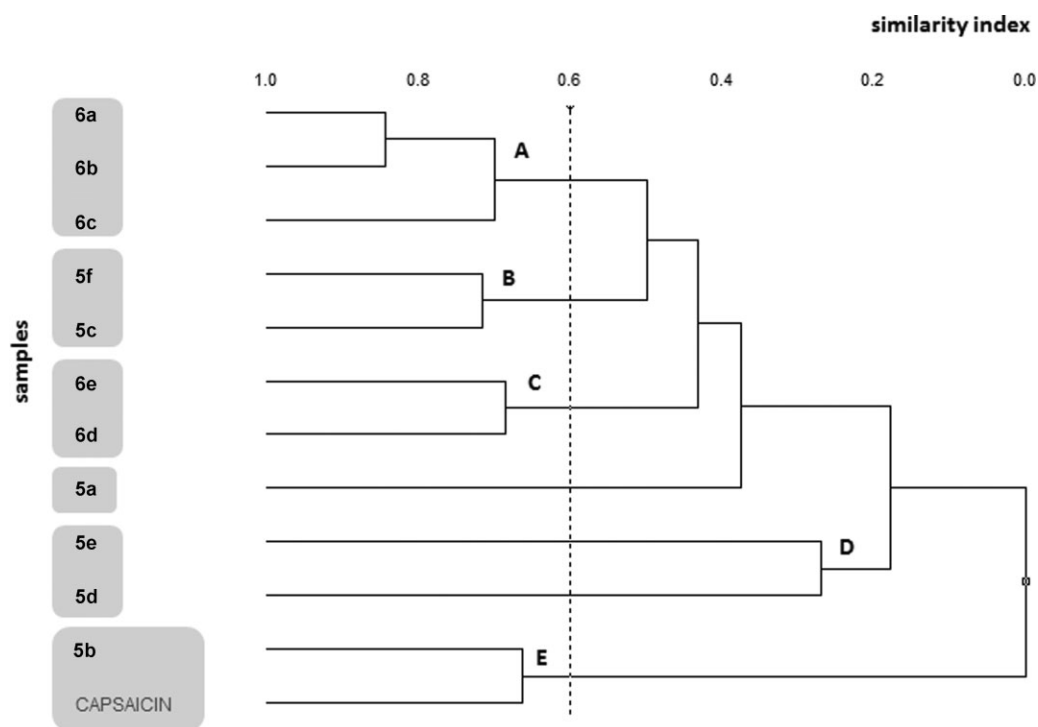


Figure 4. Dendrogram found for HCA of samples. Considering a similarity cursor of 0.6 (dotted line), capsaicin derivatives were grouped into four sub-clusters: A (68.8% similarity), B (69.8% similarity), C (66.3% similarity), and E (64.1% similarity). The clusters were basically formed regarding the isosteric group (amide or ester) and nature of side chain (alkyl or aryl).

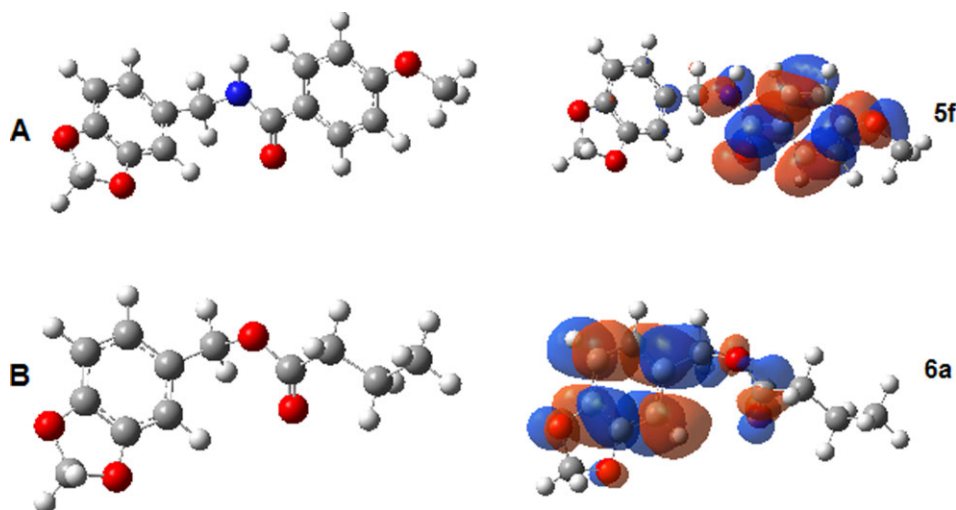


Figure 5. LUMO map found for compounds **5f** (A) and **6a** (B). Color ranges from -0.02 (intense red) to 0.02 (intense blue) (GaussView 3.0) [28]. The compounds are represented as ball and stick model. The carbon atoms are in gray, nitrogen in blue, hydrogen in white, and oxygen atoms are in red.

chains (capsaicin and **5b**). Compound **5a**, a short side chain amide, was not grouped into any clusters when a similarity cursor of 60% was considered. The same behavior was observed for compounds **5e** and **5d** (cluster D; 21.5% similarity), which contain electron withdrawing substituents (3-NO_2 , $3,4\text{-Cl}$).

It is well known that molecular properties are directly dependent upon the chemical structure. Steric properties (including geometric and topological properties), for instance, are related to the molecular shape. Electronic and stereo chemical properties can be considered as the most important requirements in the molecular recognition process. Regarding PCA findings, among the highest loading values (in module) are a topological descriptor (Randic index), in PC1, and an electronic descriptor as frontier molecular orbital energy (E_{lumo}), in PC2. This electronic property can be graphically visualized through the LUMO map distribution. The LUMO maps for compounds **5f** (active) and **6a** (inactive) are displayed in Fig. 5. The active compound **5f** had a 10-fold more negative value of E_{lumo} (-20.90 kcal/mol) than **6a** (-2.13 kcal/mol). Additionally, the LUMO map distribution was in opposite regions regarding the two molecules, corroborating with the experimental findings.

Conclusions

A series of twelve novel benzo[d][1,3]dioxol-5-ylmethyl functional analogues of capsaicin were designed through LBDD strategy, synthesized in a facile acylation method, and experimentally evaluated. Three compounds (**5f**, **6c**, and **6e**) exhibited significant *in vitro* cytotoxicity at micromolar (μM)

range against B16F10, SK-MEL-28 and NCI-H1299 cell lines. The chemometric study (PCA and HCA) has revealed interesting points regarding structure–property relationships. PCA findings indicated that topological (Randic index) and electronic properties (E_{lumo}) might be important for improving the biological activity. The investigated set of bioisoster molecules can be considered as promising scaffolds to be explored. Indeed, new substituted aryl/alkyl amides and esters are going to be synthesized in order to obtain potential, selective and non-toxic anticancer agents, particularly against melanoma and lung cancer.

Experimental

Chemistry

All reagents used are of analytical grade having $>97\%$ purity. For the chemical synthesis and analysis of capsaicin analogues the following compounds were used: Piperonylamine, piperonyl alcohol, propionic acid, butanoic acid, hexanoic acid, nonanoic acid, isovaleric acid, benzoic acid, 4-methylbenzoic acid, 3,4-chlorobenzoic acid, 4-methoxybenzoic acid, 3-nitrobenzoic acid, and oxalyl chloride (Sigma-Aldrich Inc., St. Louis, MO, USA). Melting points were recorded on a Buchi M-565 apparatus and were uncorrected. TLC was carried out using silica gel plates (TLC silica gel 60 F_{254} aluminum sheets, Merck Darmstadt, Germany) and the spots were visualized under UV light at 254 nm. Flash chromatography was performed for purification of the compounds on silica gel 60 (70–230 mesh ASTM) (Merck Darmstadt). The structure of each compound was confirmed by ^1H NMR, ^{13}C NMR and elemental analysis. ^1H and ^{13}C NMR spectra were recorded on Bruker AC-300 at 300 and 75 MHz, respectively, and chemical shifts were expressed as δ units, using tetramethylsilane (TMS) as an internal standard. The spectral splitting patterns were described as follows: s, singlet; d, doublet; dd, double doublet;

ddd, double double doublet; t, triplet; m, multiplet; bs, broad singlet, and bt, broad triplet peak.

General procedure for the synthesis of compounds **5a–f** and **6a–e**

In different 100 mL flasks, the carboxylic acids **3a–j** (5 mmol) were dissolved in dichloromethane (CH₂Cl₂) (50 mL). Next, oxalyl chloride (0.63 g, 458 µL, 5 mmol) and three drops of *N,N*-dimethylformamide were added. The resulting solution was stirred at room temperature for 2 h. Subsequently, the excess of oxalyl chloride was removed under high vacuum and the second step was performed in one pot through the addition of 10 mL of CH₂Cl₂, **1** (622 µL, 0.755 g, 5 mmol) (**5a–f** synthesis) or **2** (0.760 g, 5 mmol) (**6a–e** synthesis), triethylamine (Et₃N) (723 µL, 0.525 g, 5.2 mmol), and 4-dimethylaminopyridine (DMAP) (catalytic). The reaction mixture was stirred for 4 h under nitrogen atmosphere at 0 °C. The organic layer was washed with 5% HCl aqueous solution, water, brine and dried over MgSO₄. The solvent was removed under high vacuum and the products were purified by flash column chromatography with hexanes/ethyl acetate system as solvent.

N-(Benzo[d][1,3]dioxol-5-ylmethyl)propionamide (**5a**)

Yield: 68%; White solid, m.p. 97–98 °C; ¹H NMR (CDCl₃; 300 MHz) δ: 6.77 (3H, m, 4, 5, 7-ArH), 5.97 (2H, s, 1-OCH₂O–), 5.63 (1H, bs, 9-NH), 4.37 (2H, d, 8-CH₂), 2.26 (2H, q, *J* = 7.6 Hz, 11-CH₂), 1.20 (3H, t, *J* = 7.6 Hz, 12-CH₃); ¹³C NMR (CDCl₃, 75 MHz) δ: 173.5 (C10), 147.9 (C3), 147.0 (C2), 132.3 (C6), 121.1 (C7), 108.4 (C4), 108.3 (C5), 101.1 (C1), 43.4 (C8), 29.7 (C11), 9.8 (C12). Anal. calcd. for C₁₁H₁₃O₃N: C, 63.76; H, 6.32; N, 6.76. Found: C, 63.82; H, 6.41; N, 6.58.

N-(Benzo[d][1,3]dioxol-5-ylmethyl)nonanamide (**5b**)

Yield: 70%; White solid, m.p. 90–91 °C; ¹H NMR (CDCl₃; 300 MHz) δ: 6.77 (3H, m, 4, 5, 7-ArH), 5.96 (2H, s, 1-OCH₂O–), 5.70 (1H, bs, 9-NH), 4.36 (2H, d, 8-CH₂), 2.21 (2H, t, *J* = 7.6 Hz, 11-CH₂), 1.68 (2H, m, 12-CH₂), 1.30 (10H, m, 13, 14, 15, 16, 17-CH₂), 0.90 (3H, t, *J* = 6.7 Hz, 18-CH₃); ¹³C NMR (CDCl₃, 75 MHz) δ: 172.9 (C10), 147.9 (C3), 147.0 (C2), 132.4 (C6), 121.1 (C7), 108.3 (C4), 108.3 (C5), 101.1 (C1), 43.4 (C8), 36.8 (C11), 31.8 (C12), 29.3 (C13), 29.3 (C14), 29.1 (C15), 25.7 (C16), 22.6 (C17), 14.0 (C18). Anal. calcd. for C₁₇H₂₅O₃N: C, 70.07; H, 8.65; N, 4.81. Found: C, 69.83; H, 8.72; N, 4.81.

N-(Benzo[d][1,3]dioxol-5-ylmethyl)-4-methylbenzamide (**5c**)

Yield: 72%; White crystal, m.p. 131–132 °C; ¹H NMR (DMSO-*d*₆; 300 MHz) δ: 8.87 (1H, bt, *J* = 5.8 Hz, 9-NH), 7.79 (2H, d, *J* = 8.2 Hz, 12, 13-ArH), 7.27 (2H, d, *J* = 8.2 Hz, 14, 15-ArH), 6.83 (3H, m, 4, 5, 7-ArH), 5.98 (2H, s, 1-OCH₂O–), 4.38 (2H, d, 8-CH₂), 2.36 (3H, s, 17-CH₃); ¹³C NMR (DMSO-*d*₆, 75 MHz) δ: 165.9 (C10), 147.2 (C3), 146.0 (C2), 141.0 (C16), 133.7 (C11), 131.7 (C6), 128.8 (C14, C15), 127.2 (C12, C13), 120.4 (C7), 107.9 (C5), 107.9 (C4), 100.7 (C1), 42.4 (C8), 21.0 (C17). Anal. calcd. for C₁₆H₁₅O₃N: C, 71.36; H, 5.61; N, 5.20. Found: C, 71.30; H, 5.74; N, 5.17.

N-(Benzo[d][1,3]dioxol-5-ylmethyl)-3,4-dichlorobenzamide (**5d**)

Yield: 60%; White solid, m.p. 125–126 °C; ¹H NMR (DMSO-*d*₆; 300 MHz) δ: 9.13 (1H, bt, *J* = 5.8 Hz, 9-NH), 8.12 (1H, d, *J* = 2.0 Hz, 13-ArH), 7.86 (1H, dd, *J* = 8.4 Hz, *J* = 2.1 Hz, 12-ArH), 7.76 (1H, d,

J = 8.4 Hz, 14-ArH), 6.85 (3H, m, 4, 5, 7-ArH), 5.98 (2H, s, 1-OCH₂O–), 4.38 (2H, d, *J* = 5.9 Hz, 8-CH₂); ¹³C NMR (DMSO-*d*₆, 75 MHz) δ: 163.8 (C10), 147.2 (C3), 146.1 (C2), 134.6 (C16), 134.0 (C11), 133.0 (C15), 131.2 (C14), 130.7 (C13), 129.2 (C12), 127.6 (C6), 120.6 (C7), 108.0 (C4), 108.0 (C5), 100.8 (C1), 42.7 (C8). Anal. calcd. for C₁₅H₁₁O₃NCl₂: C, 55.58; H, 3.42; N, 4.32. Found: C, 55.46; H, 3.53; N, 4.28.

N-(Benzo[d][1,3]dioxol-5-ylmethyl)-3-nitrobenzamide (**5e**)

Yield: 63%; Yellow solid, m.p. 111–112 °C; ¹H NMR (DMSO-*d*₆; 300 MHz) δ: 8.60 (1H, t, 13-ArH), 8.37 (1H, ddd, 16-ArH), 8.19 (1H, m, 12-ArH), 7.66 (1H, t, 14-ArH), 6.84 (3H, m, 4, 5, 7-ArH), 6.58 (1H, bs, 9-NH), 5.97 (2H, s, 1-OCH₂O–), 4.59 (2H, d, *J* = 5.6 Hz, 8-CH₂); ¹³C NMR (DMSO-*d*₆, 75 MHz) δ: 164.8 (C10), 148.2 (C15), 148.1 (C3), 146.4 (C2), 136.0 (C11), 133.3 (C12), 131.3 (C6), 129.9 (C14), 126.1 (C16), 121.7 (C13), 121.5 (C6), 108.6 (C4), 108.5 (C5), 101.2 (C1), 44.3 (C8). Anal. calcd. for C₁₅H₁₂N₂O₅: C, 60.00; H, 4.03; N, 9.33. Found: C, 59.83; H, 3.79; N, 9.02.

N-(Benzo[d][1,3]dioxol-5-ylmethyl)-4-methoxybenzamide (**5f**)

Yield: 73%; White solid, m.p. 113–114 °C; ¹H NMR (CDCl₃; 300 MHz) δ: 7.74 (2H, d, *J* = 8.9 Hz, 12, 13-ArH), 6.91 (2H, d, *J* = 8.9 Hz, 14, 15-ArH), 6.81 (3H, m, 4, 5, 7-ArH), 6.33 (1H, bt, 9-NH), 5.94 (2H, s, 1-OCH₂O–), 4.52 (2H, d, *J* = 5.6 Hz, 8-CH₂), 3.84 (3H, s, 14-OCH₃); ¹³C NMR (CDCl₃, 75 MHz) δ: 166.8 (C10), 162.3 (C16), 148.0 (C3), 147.0 (C2), 132.3 (C12, C13), 128.8 (C6), 126.7 (C11), 121.2 (C7), 113.8 (C14, C15), 108.5 (C4), 108.3 (C5), 101.1 (C1), 55.4 (C17), 43.9 (C8). Anal. calcd. for C₁₆H₁₅NO₄: C, 67.36; H, 5.30; N, 4.91. Found: C, 66.86; H, 5.53; N, 4.84.

Benzo[d][1,3]dioxol-5-ylmethyl butanoate (**6a**)

Yield: 63%; Yellow liquid; ¹H NMR (CDCl₃; 300 MHz) δ: 6.80 (3H, m, 4, 5, 7-ArH), 5.95 (2H, s, 1-OCH₂O–), 5.01 (2H, s, 8-CH₂), 2.31 (t, 2H, *J* = 7.4 Hz, 11-CH₂), 1.66 (m, 2H, *J* = 7.4 Hz, 14.9 Hz, 12-CH₂), 0.84 (t, 3H, 14.8 Hz, 13-CH₃); ¹³C NMR (CDCl₃, 75 MHz) δ: 173.4 (C10), 147.8 (C3), 147.6 (C2), 130.0 (C6), 122.1 (C7), 108.9 (C4), 108.2 (C5), 101.1 (C1), 66.0 (C8), 36.2 (C11), 18.4 (C12), 13.6 (C13). Anal. calcd. for C₁₂H₁₄O₄: C, 64.85; H, 6.35. Found: C, 64.85; H, 6.35.

Benzo[d][1,3]dioxol-5-ylmethyl 3-methyl butanoate (**6b**)

Yield: 70%; Yellow liquid; ¹H NMR (CDCl₃; 300 MHz) δ: 6.80 (3H, m, 4, 5, 7-ArH), 5.94 (2H, s, 1-OCH₂O–), 5.00 (2H, s, 8-CH₂), 2.15 (m, 3H, 11,12-CH₂), 0.94 (d, 6H, 13,14-CH₂); ¹³C NMR (CDCl₃, 75 MHz) δ: 172.9 (C10), 147.8 (C3), 147.6 (C2), 130.0 (C6), 122.2 (C7), 109.0 (C4), 108.2 (C5), 101.1 (C1), 65.9 (C8), 43.4 (C11), 25.7 (C12), 22.4 (C13, C14). Anal. calcd. for C₁₃H₁₆O₄: C, 66.09; H, 6.83. Found: C, 65.85; H, 6.71.

Benzo[d][1,3]dioxol-5-ylmethyl hexanoate (**6c**)

Yield: 68%; Yellow liquid; ¹H NMR (CDCl₃; 300 MHz) δ: 6.85 (2H, d, *J* = 7.4 Hz, 4, 5-ArH), 6.80 (1H, d, *J* = 7.4 Hz, 7-ArH), 5.97 (2H, s, 1-OCH₂O–), 5.03 (2H, s, 8-CH₂), 2.35 (2H, t, *J* = 7.5 Hz, 11-CH₂), 1.66 (2H, m, 12-CH₂), 1.33 (4H, m, 13,14-CH₂), 0.91 (3H, t, 15-CH₃); ¹³C NMR (CDCl₃, 75 MHz) δ: 173.5 (C10), 147.8 (C3), 147.6 (C2), 130.0 (C6), 122.1 (C7), 108.9 (C4), 108.2 (C5), 101.1 (C1), 66.0 (C8), 34.3 (C11), 31.3 (C12), 24.6 (C13), 22.3 (C14), 13.8 (C15). Anal. calcd. for C₁₄H₁₈O₄: C, 67.18; H, 7.25. Found: C, 67.54; H, 7.46.

Benzo[d][1,3]dioxol-5-ylmethyl benzoate (6d)

Yield: 74%; White solid, m.p. 63–64°C; ^1H NMR (CDCl_3 ; 300 MHz) δ : 7.98 (2H, d, $J = 7.6$ Hz, 12, 13-ArH), 7.48 (1H, t, $J = 7.6$, 16-ArH), 7.35 (2H, t, $J = 7.6$ Hz, 14, 15-ArH), 6.85 (2H, d, 4, 5-ArH), 6.73 (1H, d, 7-ArH), 5.89 (2H, s, 1- OCH_2O -), 5.19 (2H, s, 8- CH_2); ^{13}C NMR (CDCl_3 , 75 MHz) δ : 166.4 (C10), 147.9 (C3), 147.7 (C2), 133.0 (C16), 130.2 (C6), 129.9 (C11), 129.7 (C14, C15), 128.4 (C12, C13), 122.2 (C7), 109.0 (C4), 108.3 (C5), 101.2 (C1), 66.7 (C8). Anal. calcd. for $\text{C}_{15}\text{H}_{12}\text{O}_4$: C, 70.31; H, 4.72. Found: C, 70.24; H, 4.93.

Benzo[d][1,3]dioxol-5-ylmethyl 3,4-dichlorobenzoate (6e)

Yield: 61%; White solid, m.p. 98–99°C; ^1H NMR ($\text{DMSO}-d_6$; 300 MHz) δ : 8.07 (1H, d, $J = 2.0$ Hz, 13-ArH), 7.90 (1H, dd, $J = 2.0$ Hz, $J = 8.4$ Hz, 12-ArH), 7.78 (1H, d, $J = 8.4$ Hz, 14-ArH), 7.06 (1H, d, $J = 1.5$ Hz, 4-ArH), 6.98 (1H, dd, $J = 7.9$ Hz, $J = 1.5$ Hz, 7-ArH), 6.91 (1H, d, $J = 7.9$ Hz, 5-ArH), 6.03 (2H, s, 1- OCH_2O -), 5.25 (2H, s, 8- CH_2); ^{13}C NMR ($\text{DMSO}-d_6$, 75 MHz) δ : 163.8 (C10), 147.4 (C3), 147.3 (C2), 136.3 (C16), 131.7 (C11), 131.2 (C6), 130.8 (C14), 130.1 (C13), 129.2 (C15), 129.2 (C12), 122.3 (C7), 109.0 (C4), 108.1 (C5), 101.1 (C1), 66.9 (C8). Anal. calcd. for $\text{C}_{15}\text{H}_{10}\text{O}_4\text{Cl}_2$: C, 55.41; H, 3.10. Found: C, 55.58; H, 3.29.

Cytotoxic activity

All cell lines studied were purchased from the American Type Tissue Culture Collection (ATCC, Rockville, MD, USA). Murine melanoma (B16F10), human melanoma (SK-MEL-28), non-small cell lung cancer (NCI-H1299 and NCI-H460), breast adenocarcinoma (SK-BR-3 and MDA-MB-231), and human fetal lung fibroblast (MRC-5), were routinely cultured in Modified Dulbecco's Medium or RPMI supplemented with 2 mM L-glutamine, 5% (v/v) FCS and maintained at 37°C in 95% humidified atmosphere, containing 5% CO_2 . Asynchronous cell cultures in the exponential phase of growth.

Cytotoxicity activities of compounds **5a–f**, **6a–e**, and capsaicin were evaluated against seven different cell lines. Cells were plated in 96-well plates at a concentration of 1×10^4 cells per well. The cells were allowed to grow for 24 h, then, treated with the compounds **5a–f**, **6a–e**, or capsaicin, at concentration of 200, 175, 150, 100, and 50 μM . After 24 h of treatment, cell viability was determined by MTT (3-(4,5-dimethylthiazol-2-yl)-2,5-diphenyltetrazolium bromide) (Sigma, St Louis, MO, USA) [29]. Briefly, MTT solution (20 μL) was added to each well (final concentration = 0.5 mg/mL) and the plate was incubated for additional 3 h. Finally, DMSO (200 μL) was added to each well, and the absorbance was measured in a plate reader (Thermoplate Q4 TP Reader, Tokay Hit, Japan) at 540 nm. The 50% inhibitory concentration (IC_{50}) values were calculated using a proper analysis (non-linear regression-curve fit). Each experiment was performed using six replicates for each compound concentration, and repeated in triplicate.

Molecular modeling approach

The three-dimensional (3D) molecular models of capsaicin and its derivatives were built up, in their neutral forms, using the HyperChem 7.0 MM + force field [30] without any constraints. The crystal data from 3-chloro-N-(4-hydroxy-3-methoxy-benzyl)-2,2-diethylpropanamide [31] was employed as the starting geometry for capsaicin and N-[(1,3-benzodioxol-5-yl)methyl]-4-methylbenzamide [32] for compounds **5a–f** and **6a–e**. Partial atomic charges were computed with AM1 semi-empirical method [33], also

implemented in HyperChem 7.0 [30]. The MOLSIM 3.2 software [34] was used to perform energy-minimization (steepest descent and conjugate gradient methods; convergence criterion of 0.01 kcal/mol) and molecular dynamics (MD) simulations. MD simulations of 1 ns (step size of 1 fs) at 310 K were performed for each molecular model. Dielectric constant of 3.5 was used to simulate the environment of biological membranes and enzyme or receptor binding sites [35]. It was assigned a fictitious atomic mass of 5000 u.m.a. to some atoms position in order to maintain the structural integrity of the molecular models during simulation. Output trajectory file was recorded every 20 ps steps resulting in a conformational ensemble profile (CEP) of 50,000 conformers for each investigated molecule. After equilibration, conformers were selected, for each 100 ps, in order to find the lowest-energy conformation more frequent. Then, care was taken in the conformation selection process. The intramolecular solvation and hydrogen bonding energy contributions were computed for each selected conformer from MD simulations scheme. The hydration shell model proposed by Forsythe and Hopfinger [36] was employed to estimate the solvation energy contribution. Total potential energy (E_{TOT}) of each selected conformation corresponds to the summation of the following intramolecular energy contributions: stretching (E_{STRETCH}), bending (E_{BEND}), torsional (E_{TORS}), Lennard-Jones or 1–4 interactions ($E_{1,4}$), van der Waals (E_{vdw}), electrostatic (E_{CHARGE}), hydrogen bonding (E_{HB}), and solvation (E_{SOLV}).

The lowest-energy conformation of each molecule from MD simulations was energy-minimized [34] and, subsequently, used as starting geometry to calculate physicochemical and structural properties of distinct nature (thermodynamic, hydrophobic, electronic, topological, geometric, and steric), which were explored in this study. Electronic properties, such as partial atomic charges from electrostatic potentials using a grid based method (CHELPG) [37], dipole moment (μ) (total and x, y, z) and frontier molecular orbital energies (E_{HOMO} , energy of the highest occupied molecular orbital; E_{LUMO} , energy of the lowest unoccupied molecular orbital), were computed with the B3LYP (Becke, three-parameter, Lee–Yang–Parr) [38] hybrid functional and 6-31(d,p) basis [39].

MarvinView program [40] was used to calculate steric, topological/geometric, and lipophilic properties. ClogP was calculated by the weighted method, assigning equal weight for each method [41–43]. Further detailed information regarding all descriptors, methods, and respective software used to perform these calculations are listed in the Supplementary Information (Table S1).

A table containing 12 rows, which correspond to the samples (analogues) and capsaicin, and 48 columns, which correspond to the descriptors or calculated molecular properties (see Supplementary Information, Table S2), was used as input for the exploratory data analysis. Due to distinct magnitude orders among the calculated variables, an autoscaling procedure was applied as a preprocessing method [22].

Exploratory data analysis

The exploratory data analysis, which comprises the principal component analysis (PCA) and hierarchical cluster analysis (HCA) was carried out employing the Pirouette 3.11 software [27].

Principal component analysis (PCA)

PCA is a data compression method based upon the correlation among variables or descriptors. Its purpose is to reduce the

dimensionality of a data set by grouping the correlated variables and replacing the original descriptors with a new set called factors or principal components (PCs), onto which the data is projected. PCs or factors are completely uncorrelated variables built up as simple linear combinations from the original variables, containing most of the variability in the data set even though in a much lower dimensional space.

The data matrix $X(I \times J)$ corresponding to I compounds and J descriptors, was decomposed into two matrices, T and L , such that $X = TL^T$. The T matrix, which is known as the score matrix, represents the positions of the compounds in the new coordinate system where the PCs are the axes. Scores are integral to exploratory analysis because they show intersample relationships. L is the matrix of loadings whose columns describe how the new axes (the PCs) are built from the old axes, and indicates the variables contribution to each PC [20, 21, 27]. In this exploratory data analysis, PCA was run up to ten factors or PCs. The outliers' diagnosis, implemented in Pirouette 3.11 software, was also performed through the Mahalanobis distance [26].

Hierarchical cluster analysis (HCA)

HCA was also carried out using the Pirouette 3.11 program, employing the complete linkage method and Euclidean distance. In HCA, distances between pairs of samples (or variables) are calculated and compared. When distances between samples are relatively small, this implies that the samples are similar. The distances between samples or variables were calculated and transformed into a similarity matrix whose elements correspond to the similarity indexes. The similarity scale ranges from zero to one, and the larger the similarity index, the smaller is the distance between any pair of samples or variables [20]. Results were expressed as a dendrogram, which is a tree-shaped map constructed from the distances data.

The authors have declared no conflict of interest.

References

- [1] Y. L. N. Murthy, K. P. Suhasini, A. S. Pathania, S. Bhushan, Y. Nagendra Sastry, *Eur. J. Med. Chem.* **2013**, 62, 545–555.
- [2] B. M. Ivković, K. Nikolic, B. B. Ilić, Ž. S. Žižak, R. B. Novaković, O. A. Čudina, S. M. Vladimirov, *Eur. J. Med. Chem.* **2013**, 63, 239–255.
- [3] S. N. Baytas, N. Inceler, A. Yilmaz, *Med. Chem. Res.* **2013**, 22, 4893–4908.
- [4] X. Yang, Q. Shi, C.-Y. Lai, C.-Y. Chen, E. Ohkoshi, S.-C. Yang, C.-Y. Wang, K. F. Bastow, T.-S. Wu, S.-L. Pan, C.-M. Teng, P.-C. Yang, K.-H. Lee, *J. Med. Chem.* **2012**, 55, 6751–6761.
- [5] V. Castro-Castillo, C. Suárez-Rozas, N. Castro-Loiza, C. Theoduloz, B. K. Cassels, *Eur. J. Med. Chem.* **2013**, 62, 688–692.
- [6] S. W. Fesik, *Nat. Rev. Cancer* **2005**, 5, 876–885.
- [7] N. N. Danial, S. J. Korsmeyer, *Cell* **2004**, 116, 205–219.
- [8] S.-P. Huang, J.-C. Chen, C.-C. Wu, C.-T. Chen, N.-Y. Tang, Y.-T. Ho, C. Lo, J.-P. Lin, J.-G. Chung, J.-G. Lin, *Anticancer Res.* **2009**, 29, 165–174.
- [9] K. Ito, T. Nakazato, K. Yamato, Y. Miyakawa, T. Yamada, N. Hozumi, K. Segawa, Y. Ikeda, M. Kizaki, *Cancer Res.* **2004**, 64, 1071–1078.
- [10] J. Y. Kim, E. H. Kim, S. U. Kim, T. K. Kwon, K. S. Choi, *Carcinogenesis* **2010**, 31, 367–375.
- [11] A. M. Sánchez, S. Malagarie-Cazenave, N. Olea, D. Vara, A. Chiloeches, I. Díaz-Laviada, *Apoptosis* **2007**, 12, 2013–2024.
- [12] N. H. Thoennissen, J. O'Kelly, D. Lu, G. B. Iwanski, D. T. La, S. Abbassi, A. Leiter, B. Karlan, R. Mehta, H. P. Koeffler, *Oncogene* **2010**, 29, 285–296.
- [13] C.-C. Wu, J.-P. Lin, J.-S. Yang, S.-T. Chou, S.-C. Chen, Y.-T. Lin, H.-L. Lin, J.-G. Chung, *Mutat. Res.* **2006**, 601, 71–82.
- [14] M.-J. Ludy, G. E. Moore, R. D. Mattes, *Chem. Senses* **2012**, 37, 103–121.
- [15] P. L. de-Sá-Júnior, K. F. M. Pasqualoto, A. K. Ferreira, M. T. Tavares, M. C. F. C. B. Damião, R. A. de Azevedo, D. A. D. Câmara, A. Pereira, D. M. Souza, R. P. Filho, *Toxicol. Appl. Pharmacol.* **2013**, 266, 385–398.
- [16] G. A. Patani, E. J. LaVoie, *Chem. Rev.* **1996**, 96, 3147–3176.
- [17] W. C. Black, C. I. Bayly, D. E. Davis, S. Desmarais, J.-P. Falguyet, S. Léger, C. S. Li, F. Massé, D. J. MacKay, J. T. Palmer, M. D. Percival, J. Robichaud, N. Tsou, R. Zamboni, *Bioorg. Med. Chem. Lett.* **2005**, 15, 4741–4744.
- [18] A. C. L. Leite, K. P. da Silva, I. a Souza, J. M. de Araújo, D. J. Brondani, *Eur. J. Med. Chem.* **2004**, 39, 1059–1065.
- [19] Y. You, *Curr. Pharm. Des.* **2005**, 11, 1695–1717.
- [20] M. M. C. Ferreira, *J. Braz. Chem. Soc.* **2002**, 13, 742–753.
- [21] M. B. Beebe, K. R. Pell, R. J. Seasholtz, *Chemometrics: A Practical Guide*, Wiley-Interscience, New York **1998**.
- [22] M. M. F. Ferreira, A. M. Antunes, M. S. Melgo, P. L. O. Volpe, *Quim. Nova* **1999**, 2, 724–731.
- [23] M. L. D. C. Barbosa, L. M. Lima, R. Tesch, C. M. R. Sant'anna, F. Totzke, M. H. G. Kubbutat, C. Schachtele, S. A. Laufer, E. J. Barreiro, *Eur. J. Med. Chem.* **2013**, 71, 1–14.
- [24] T. Inoue, M. Morita, T. Tojo, A. Nagashima, A. Moritomo, H. Miyake, *Bioorg. Med. Chem.* **2013**, 21, 3873–3881.
- [25] J. B. Cross, D. C. Thompson, B. K. Rai, J. C. Baber, K. Y. Fan, Y. Hu, C. Humblet, *J. Chem. Inf. Model.* **2009**, 49, 1455–1474.
- [26] P. C. Mahalanobis, On the generalized distance in statistics, in: *Proceedings of the National Institute of Sciences of India*, in: New Delhi, **1936**.
- [27] Pirouette 3.11, Infometrix Inc, Woodinville, WA, **1990–2003**.
- [28] Gaussview 3.0, Gaussian Inc, Pittsburgh, PA, **2000–2003**.
- [29] T. Mosmann, *J. Immunol. Methods* **1983**, 65, 55–63.
- [30] Hyperchem Program Release 7 for Windows, Hypercube, Inc, Gainesville, FL, **2002**.
- [31] Y.-L. Huang, W.-L. Wang, S. Shan, *Acta Crystallogr. Sect. E* **2010**, 66, o877.
- [32] S. H. Maganhi, M. C. F. C. B. Damião, M. T. Tavares, R. Parise Filho, *Acta Crystallogr. Sect. E* **2013**, 69, o332.
- [33] M. J. S. Dewar, E. G. Zebisch, E. F. Healy, J. J. P. Stewart, *J. Am. Chem. Soc.* **1985**, 107, 3902–3909.
- [34] D. Doherty, *MOLSIM: Molecular Mechanics and Dynamics Simulation Software—User's Guide*, Version 3.2, The Chem21 Group Inc., **1997**.
- [35] J. S. Tokarski, A. J. Hopfinger, *J. Chem. Inf. Comput. Sci.* **1997**, 37, 792–811.

- [36] K. H. Forsythe, A. J. Hopfinger, *Macromolecules*, **1973**, 6, 423–437.
- [37] C. M. Breneman, K. B. Wiberg, *J. Comput. Chem.* **2004**, 11, 361–373.
- [38] A. D. Becke, *J. Chem. Phys.* **1993**, 98, 1372.
- [39] Gaussian 03W-revision B.02 for Windows, Version 6, Gaussian Inc, Pittsburgh, PA, **1995–2003**.
- [40] MarvinView 5.4.0.1-Free License, ChemAxon Ltd., **1998–2010**.
- [41] V. N. Viswanadhan, A. K. Ghose, G. R. Reysankar, R. K. Robins, *J. Chem. Inf. Comput. Sci.* **1989**, 29, 163–172.
- [42] G. Klopman, J. Li, S. Wang, M. Dimayugat, *J. Chem. Inf. Comput. Sci.* **1994**, 752–781.
- [43] PHYSPROP database. <http://www.syrres.com/what-we-do/databaseforms.aspx?id=386>.